Genome and Epigenome

Cancer Research

Long Noncoding RNA FAM225A Promotes Nasopharyngeal Carcinoma Tumorigenesis and Metastasis by Acting as ceRNA to Sponge miR-590-3p/miR-1275 and Upregulate ITGB3

Zi-Qi Zheng[1], Zhi-Xuan Li[1], Guan-Qun Zhou[1], Li Lin[1], Lu-Lu Zhang[1], Jia-Wei Lv[1], Xiao-Dan Huang[1], Rui-Qi Liu[1], FoPing Chen[1], Xiao-Jun He[1], Jia Kou[1], Jian Zhang[1,2], Xin Wen[1], Ying-Qin Li[1], Jun Ma[1], Na Liu[1], and Ying Sun[1]

Abstract

Long noncoding RNAs (lncRNA) play important roles in the tumorigenesis and progression of cancers. However, the clinical significance of lncRNAs and their regulatory mechanisms in nasopharyngeal carcinogenesis (NPC) are largely unknown. Here, based on a microarray analysis, we identified 384 dysregulated lncRNAs, of which, *FAM225A* was one of the most upregulated lncRNAs in NPC. *FAM225A* significantly associated with poor survival in NPC. N(6)-Methyladenosine (m6A) was highly enriched within *FAM225A* and enhanced its RNA stability. *FAM225A* functioned as an oncogenic lncRNA that promoted NPC cell proliferation, migration, invasion, tumor growth, and metastasis. Mechanistically, *FAM225A* functioned as a competing endogenous RNA (ceRNA) for sponging miR-590-3p and miR-1275, leading to the upregulation of their target *integrin β3* (*ITGB3*), and the activation of FAK/PI3K/Akt signaling to promote NPC cell proliferation and invasion. In summary, our study reveals a potential ceRNA regulatory pathway in which *FAM225A* modulates *ITGB3* expression by binding to miR-590-3p and miR-1275, ultimately promoting tumorigenesis and metastasis in NPC.

Significance: These findings demonstrate the clinical significance of the lncRNA *FAM225A* in nasopharyngeal carcinoma (NPC) and the regulatory mechanism involved in NPC development and progression, providing a novel prognostic indicator and promising therapeutic target.

Introduction

Nasopharyngeal carcinoma (NPC) is a unique head and neck cancer, mainly involving the epithelial lining of the nasopharynx. NPC is predominant in Southeast Asia, especially in China, accounting for 40% of new cases worldwide each year (1–3). With the combined use of magnetic resonance imaging, intensity-modulated radiotherapy and concurrent chemoradiotherapy, the prognosis of NPC patients has been substantially improved. However, approximately 30% of NPC patients eventually develop recurrence or/and distant metastasis, and the curative effect for those patients is unsatisfactory (4, 5). Therefore, advances in the identification of predictive biomarkers and clarification of underlying mechanisms are essential for the development of more individualized treatment for NPC patients.

Accurate prognostic prediction is a prerequisite for rational treatment of NPC patients, and the tumor–node–metastasis (TNM) staging system is currently considered the gold standard for guiding treatment. Based on TNM staging, NPC patients are divided into 4 stages, and receive stratified treatments accordingly. However, although NPC patients in the same stage receive similar treatment, their clinical outcomes vary. This indicates that anatomic TNM staging fails to adequately reflect the biological heterogeneity of cancer and is insufficient to accurately predict NPC patients at high risk of treatment failure. To address this limitation of TNM staging, multiple biomarkers, such as EBV-DNA, miRNA, and gene profile, have been proposed for predicting the clinical prognosis of NPC patients (6–8). However, more studies are required to identify new biomarkers and treatment targets.

Long noncoding RNAs (lncRNA) are a class of RNA molecules consisting of more than 200 nucleotides without protein-coding potential (9). Once considered transcriptional noise, lncRNAs are now known to constitute a regulatory system that functions at the transcriptional and posttranscriptional levels. LncRNAs are involved in various biological processes, such as cell proliferation, differentiation, and metastasis (10). It has been reported that dysregulation of lncRNA plays a vital role in the occurrence and development of tumors, including NPC (11–15). However, only a

[1]State Key Laboratory of Oncology in South China, Collaborative Innovation Center of Cancer Medicine, Guangdong Key Laboratory of Nasopharyngeal Carcinoma Diagnosis and Therapy, Sun Yat-sen University Cancer Center, Guangzhou, P. R. China. [2]Department of Radiation Oncology, Affiliated Cancer Hospital and Institute of Guangzhou Medical University, Guangzhou, P. R. China.

Note: Supplementary data for this article are available at Cancer Research Online (http://cancerres.aacrjournals.org/).

Z.-Q. Zheng, Z.-X. Li, G.-Q. Zhou, and L. Lin contributed equally to this article.

Corresponding Authors: Ying Sun, Sun Yat-sen University Cancer Center, State Key Laboratory of Oncology in South China, Collaborative Innovation Center for Cancer Medicine, Guangdong Key Laboratory of Nasopharyngeal Carcinoma Diagn, 651 Dongfeng Road East, Guangzhou 510060, P. R. China. Phone: 86-20-87342253; Fax: 20-87343295: E-mail: sunying@sysucc.org.cn; and Na Liu, liun1@sysucc.org.cn

Cancer Res 2019;79:4612–26

doi: 10.1158/0008-5472.CAN-19-0799

fraction of the lncRNAs in the genome have been characterized functionally (16), and the study of the functions of lncRNAs in tumorigenesis, especially in NPC, is still at an early stage. Thus, further insight into the lncRNA-dependent gene-regulatory mechanisms will provide useful prognostic biomarkers and individual treatments for NPC.

In this study, based on genome-wide microarray analysis, we identified an NPC-associated lncRNA *FAM225A*, the biological function of which in tumorigenesis has not yet been clarified. We found that high *FAM225A* expression is closely related to poor prognosis of NPC patients. The m6A mark improved the stability of methylated *FAM225A* transcripts by decreasing the RNA degradation rate, which may partially account for the upregulation of *FAM225A* in NPC. *In vitro* and *in vivo* functional experiments showed that *FAM225A* promotes NPC cell proliferation and metastasis. As a competing endogenous RNA (ceRNA), *FAM225A* sponges miR-590-3p and miR-1275 to increase *ITGB3* expression and activate the FAK/PI3K/Akt pathway. Our study elucidates the clinical significance and regulatory mechanism of *FAM225A* in NPC and provides a prognostic indicator as well as a promising therapeutic target for NPC patients.

Materials and Methods

Clinical specimens

For expression analysis, 20 freshly frozen NPC and 16 normal nasopharynx tissue samples were obtained from the Sun Yat-sen University Cancer Center. For prognosis analysis, another 206 paraffin-embedded NPC biopsy tissues were collected from NPC patients with detailed clinical characteristics and long-term follow-up data at the Sun Yat-sen University Cancer Center (China) from January 2006 to December 2009. All of the patients were diagnosed with nonmetastatic NPC, without receiving any antineoplastic therapy prior to biopsy. This study was approved by the Institutional Ethical Review Board of the Sun Yat-sen University Cancer Center (GZR2018-030), and written informed consent was obtained from all patients.

Cell culture

Nine NPC cell lines (CNE-1, CNE-2, HONE-1, SUNE-1, HNE-1, 5-8F, 6-10B, C666-1, and HK-1) were maintained in RPMI-1640 (Invitrogen) supplemented with 10% fetal bovine serum (FBS; Gibco), and the other 2 NPC cell lines (S18 and S26) were cultured in DMEM (Invitrogen) supplemented with 10% FBS. The human immortalized nasopharyngeal epithelial cell lines (NP69 and N2Tert) were cultured in keratinocyte/serum-free medium (Invitrogen) supplemented with bovine pituitary extract (BD Biosciences). All cell lines that had been authenticated were generously provided by Dr. M. Zeng (Sun Yat-sen University Cancer Center). In addition, the 293T cells obtained from the ATCC were cultured in DMEM supplemented with 10% FBS.

Microarray analysis

LncRNA expression was analyzed using the Arraystar Human LncRNA Microarray v3.0 by KangChen Bio-tech as previously described (17). The GeneSpring GX v12.1 software package (Agilent Technologies) was used for data normalization and subsequent processing. Differentially expressed lncRNAs were identified using a stringent filtering criteria (fold change ≥ 2, $P < 0.05$). Heat map and volcano plots were generated with the "pheatmap" and "ggplot2" packages in R (version 3.4.4). The microarray data have been deposited in the National Center for Biotechnology Information's Gene-Expression Omnibus (accession number GSE126683).

RNA extraction, reverse transcription, and real-time RT-PCR

Total RNA from cell lines and freshly frozen tissues or paraffin-embedded tissues were isolated by TRIzol reagent (Invitrogen) or the QIAGEN FFPE RNeasy kit (QIANGEN). Reverse transcription was performed using M-MLV reverse transcriptase (Promega) with Bulge-Loop miRNA-specific RT primers (RiboBio) for miRNA or random primers (Promega) for mRNA and lncRNA. The Platinum SYBR Green qPCR SuperMix-UDG reagents (Invitrogen) were used in quantitative RT-PCR analysis with the Bio-Rad CFX96 Touch sequence detection system (Bio-Rad Laboratories Inc.). GAPDH or U6 was used as an endogenous control for normalization. All primer sequences are listed in Supplementary Table S1. The relative fold changes in expression were analyzed using the $2^{-\Delta\Delta CT}$ method.

m6A RNA methylation quantification

Total m6A levels of the extracted RNA were measured by the EpiQuik m6A RNA Methylation Quantification Kit (Colorimetric; Epigentek) according to the manufacturer's instructions. Poly-A-purified RNA (200 ng) was used for each sample analysis.

RNA immunoprecipitation

The EZ-Magna RIP kit (Millipore) was used for RNA immunoprecipitation (RIP) according to the manufacturer's instructions. Briefly, 24 hours after transfection, cells were harvested to perform RIP experiments using an m6A antibody (2 μg/sample; Synaptic Systems) or Ago2 antibody (5 μg/sample; Abcam). IgG was used as a negative control. The coprecipitated RNAs were then detected by quantitative RT-PCR as previously described. When analyzing RIPed RNA, a comparative Ct ($\Delta\Delta C_t$) method was used. The input fraction Ct value was used to normalize the RNA sample preparation differences in each group, and the negative controls (IgG) C_t was used to adjust background fraction. The primers used for the measurement of m6A-modified *FAM225A* levels or detecting *FAM225A* involved in the RNA-induced silencing complex (RISC) are provided in Supplementary Table S1.

Gene set enrichment analysis

The gene set enrichment analysis (GSEA) software (version 3.0, www.broadinstitute.org/
gsea/) was used to identify gene signatures between groups with high (top 25%, $n = 8$) and low (bottom 25%, $n = 8$) *FAM225A* expression based on the GSE12452 data set (Supplementary Table S2). The results of GSEA are expressed using normalized enrichment scores that take into account the size and degree of overrepresentation of the gene set at the top or bottom of the aligned gene list [$P < 0.05$ and false discovery rate (FDR) ≤ 0.25].

Transient transfection and generation of stably transfected cell lines

The shRNAs against *FAM225A* or *integrin β3* (*ITGB3*) were synthesized according to the sequences shown in Supplementary Table S3. The coding sequence of *FAM225A* was synthesized by GENEWIZ and cloned into the lentiviral plasmid pSin-EF2-puromycin (Addgene). The pENTER-*ITGB3* plasmid and pENTER-vector were purchased from Vigene Biosciences. The miR-590-3p or miR-1275 mimics, inhibitor, and negative

controls were purchased from RiboBio (Supplementary Table S4). Cells were transfected using Lipofectamine 3000 reagent (Invitrogen) or RNAiMAX Reagent (Invitrogen). The cells were harvested for assays at 48 hours after transfection.

The shRNA-*FAM225A* 2# or control scrambled shRNA was inserted into pLKO.1 vector, and cotransfected into 293T cells with the psPAX2 packaging plasmid (Addgene) and the pCMV-VSV-G envelope plasmid (Addgene) using polyethyleneimine (PEI; Polysciences). After transfection, the cell supernatants were harvested and used to infect SUNE-1 and HNE-1 cells, and the stably transfected cells were selected using puromycin (1 μg/mL) and validated by quantitative RT-PCR. Lentiviral plasmid overexpressing *ITGB3* (GeneCopoeia) was further transfected the selected stably cells to obtain SUNE1 cells stably coexpressing shRNA-*FAM225A* 2# and *ITGB3*.

CCK-8 and colony formation assays

For CCK-8 assays, cells were seeded into 96-well plates at a density of 1,000 cells/well, and 10 μL of CCK-8 (Dojindo) was added per well on days 0 to 5. The cells were subsequently incubated at 37°C for 2 hours, and the optical density was measured at 450 nm. For the colony formation assays, 400 cells were inoculated into 6-well plates and cultured at 37°C for 10 days. The colonies were then fixed with methanol and stained with hematoxylin.

Wound-healing, transwell migration, and invasion assays

For wound-healing assays, cells were seeded in 6-well plates and cultured to the subfusion state. After being starved in serum-free medium for 24 hours, the monolayer cells were scraped linearly to introduce an artificial wound that was captured at 0 hours and 24/48 hours. For the transwell migration and invasion assays, transwell chambers (Corning) with a membrane pore size of 8 μm were coated without or with Matrigel (BD Biosciences). Subsequently, 5×10^4 or 1×10^5 cells suspended in serum-free medium were seeded in the upper chambers, and medium supplemented with 10% FBS was placed in the lower chambers. After incubation for 12 or 24 hours, the cells were fixed, stained, and counted using an inverted microscope.

Subcellular fractionation and fluorescence *in situ* hybridization

Nuclear and cytoplasmic RNA was separated with the NE-PER Nuclear and Cytoplasmic Extraction Reagents (Invitrogen), and then analyzed by quantitative RT-PCR. For fluorescence *in situ* hybridization (FISH) assays, cells were first grown for 24 hours in 24-well plates with glass cover slips. After immobilization and permeabilization, cells were hybridized with 20 μmol/L Cy3-labeled *FAM225A* or U6 FISH probe mix (RiboBio), and 6-diamidino-2-phenylindole (DAPI) was used to stain nuclei. Images were observed with a confocal laser-scanning microscope (Olympus FV1000, Japan).

Luciferase reporter assay

The wild-type or mutant *FAM225A* fragment or *ITGB3* 3′-UTR containing the predicted binding sites of miR-590-3p or miR-1275 were subcloned into a psiCHECK2 Dual-luciferase vector (Promega). The luciferase reporter plasmids were cotransfected into NPC cells with miR-590-3p or miR-1275 mimics or the negative control. The relative luciferase activity was measured with the Dual-Luciferase Reporter Assay System (Promega) according to the manufacturer's instructions.

Biotin-labeled miRNA pulldown assay

Biotin-labeled miRNA pulldown assays were performed to identify their target RNAs (18, 19). Briefly, cells were transfected with biotin-labeled miR-590-3p or miR-1275 or miR-Ctrl (50 nmol/L), and then cell lysates were harvested 48 hours later. Simultaneously, streptavidin-Dyna beads (Invitrogen) were coated with yeast tRNA (Invitrogen) and incubated with rotation at 4°C for 2 hours. Then the beads were washed with splitting buffer and resuspended with lysis buffer. Sample lysates were mixed with precoated beads and incubated overnight at 4°C on a rotator. Beads were then pelleted to remove unbound materials and washed 5 times with ice-cold lysis buffer. RNA was isolated and subjected to quantitative RT-PCR analysis.

Western blot analysis

Cell lysates were separated by SDS-polyacrylamide gel (4%–10%) electrophoresis, and then transferred to polyvinylidene fluoride (PVDF) membranes (Millipore). The membranes were then blocked with 5% skimmed milk and incubated overnight at 4°C with the following primary detection antibodies: anti-*METTL3* (1:1,000; Abcam), anti-*ITGB3* (1:1,000; Abcam), anti-FAK (1:1,000; CST), anti-p-FAK (1:1,000; CST), anti-Akt (1:1,000; CST), anti-p-Akt (Ser-473; 1:1,000; CST), or anti-β-actin (1:5,000; Proteintech). The species-matched secondary antibodies were then incubated for 1 hour at room temperature, and the proteins were detected using BeyoECLPlus (Beyotime).

In vivo nude mouse models

All of the experimental procedures involving animals were approved by the Institutional Animal Care and Use Committee of the Sun Yat-sen University Cancer Center (L102012018070R). Female BALB/c nude mice (ages 4–5 weeks, 18–20 g) were purchased from the Charles River Laboratories. For the tumor growth model, 1×10^6 HNE1-Scrambled or HNE1-sh*FAM2225A* 2# cells were injected into the axilla of the mice, and the tumor size was measured every 3 days. On day 30, the mice were killed, and the tumors were dissected and weighed. For the lung metastasis model, SUNE1-Scrambled or SUNE1-sh*FAM2225A* 2# cells (1×10^6) were injected into the tail veins of the mice. After 8 weeks, the mice were killed and the lung tissues were fixed and paraffin-embedded for hematoxylin and eosin staining. For the inguinal lymph node metastasis model, 2×10^5 SUNE1-Scrambled or SUNE1-sh*FAM2225A* 2# cells were inoculated into the footpads of the mice. After 6 weeks, the mice were killed, and their footpad tumors and inguinal lymph nodes were detached. The sections of the inguinal lymph nodes were stained with anti-CK (pan) antibody (ZSGB-Bio) to determine whether the lymph nodes contain metastatic tumor cells, and the metastatic ratios were calculated for each group. We also constructed tumor growth model and inguinal lymph node metastasis model using SUNE1 cell that stably expressing sh-*FAM2225A* 2#, sh-*FAM2225A* 2# + *ITGB3*, or scrambled control.

In situ hybridization

An *in situ* hybridization kit (Boster Bio-Engineering Company) was used to perform *in situ* hybridization (ISH) according to the manufacturer's instructions. Briefly, after deparaffinization and rehydration, sections were digested with pepsin for 15 minutes at 37°C and subsequently dehydrated. The sections were hybridized with *FAM2225A*-specific probe (20 μL/section; Boster) or miR-590-3p/miR-1275-specific probe (2.5 μmol/L, 20 μL/section;

GeneBio) overnight at 42°C. After stringent washes and blocking, the sections were incubated with biotinylated mouse anti-digoxin antibody (Boster). Then, the sections were stained with biotinylated peroxidase, and hybridization was visualized with 3,3′-diaminobenzidine (DAB) substrate. The probe sequences of *FAM225A*, miR-590-3p, and miR-1275 were provided in Supplementary Table S5.

IHC

Sections were deparaffinized, rehydrated, and then subjected to high-pressure for antigen retrieval in EDTA antigen retrieval buffer. Endogenous peroxidase activity was inactivated by incubation with 3% hydrogen peroxide and nonspecific binding was blocked with 1% bovine serum albumin. Sections were incubated with rabbit anti-*ITGB3* monoclonal antibody (1: 400, Abcam) overnight at 4°C, and normal goat serum was used as a negative control. IHC staining was visualized using the DAKO REAL EnVision Inspection System (DAKO).

Statistical analysis

All data were presented as mean ± SD/SEM of at least 3 independent experiments. The differences between groups were assessed by the Student *t* test or χ^2 test. The Kaplan–Meier method was utilized to determine, overall, disease-free, and distant metastasis-free survival rates, and the *P* values were calculated with the long-rank test. The univariate and multivariate Cox proportional hazards models were used to analyze the effects of variables on survival. Spearman correlation analysis was used to calculate the correlation between *FAM225A* and miR-590-3p/miR-1275/*ITGB3* expression. All statistical analyses were performed using SPSS 22.0 software. All tests were two-tailed, and *P* value of <0.05 was considered to indicate statistical significance.

Results

FAM225A is overexpressed in NPC and correlates with poor clinical outcome

To identify lncRNAs involved in NPC progression, we performed genome-wide analysis of lncRNA expression in 3 pairs of NPC and normal nasopharynx tissues. We identified 384 dysregulated lncRNAs (fold change ≥2 and $P < 0.05$; Supplementary Fig. S1A and S1B), of which, *FAM225A* was one of the most highly upregulated lncRNAs in NPC (Fig. 1A; Supplementary Table S6). Additionally, *FAM225A* expression was evaluated in 20 NPC tissues and 16 normal nasopharynx tissues by quantitative RT-PCR. The results showed that *FAM225A* was significantly upregulated in freshly frozen NPC tissue samples compared with that in normal nasopharynx tissues (Fig. 1B, $P = 0.017$). Similarly, *FAM225A* expression was significantly higher in 11 NPC cell lines than that in immortalized NP69 and N2Tert cells (Fig. 1C, $P < 0.01$). Furthermore, analysis of RNA-seq data from the Cancer Genome Atlas (TCGA) showed that *FAM225A* was upregulated in 9 types of tumors (Supplementary Fig. S1C). Collectively, these results indicated that *FAM225A* overexpression is a common phenomenon in multiple tumor types, including NPC.

To investigate its clinical significance, we detected *FAM225A* expression in a cohort of 206 paraffin-embedded NPC biopsy samples using quantitative RT-PCR. All NPC patients were divided into high or low *FAM225A* expression groups using the median value as cutoff point, and statistical analysis showed that a higher *FAM225A* level was significantly associated with patients' sex, distant metastasis, and death (all $P < 0.05$; Supplementary Table S7). Furthermore, Kaplan–Meier survival analysis revealed that patients with high *FAM225A* expression had worse overall, disease-free, and distant metastasis-free survivals (Fig. 1D–F, all $P < 0.01$). Subsequently, multivariate Cox regression analyses suggested that *FAM225A* expression and TNM stage were independent prognostic factors (Supplementary Table S8).

Furthermore, we constructed a prognostic model combining *FAM225A* expression and TNM stage, and NPC patients were classified into low (*FAM225A* low expression and early TNM stage, $n = 61$), intermediate (*FAM225A* high expression or advanced TNM stage, $n = 104$) and high (*FAM225A* high expression and advanced TNM stage, $n = 41$) risk groups. Survival analysis showed significant differences in the overall, disease-free, and distant metastasis-free survival rates among the 3 patient groups (Fig. 1G–I, all $P < 0.01$). Our findings suggested that TNM stage combined with *FAM225A* expression is a promising indictor of NPC prognosis.

The m6A modification is enriched in FAM225A and improves its transcripts stability

Recently, frontier studies have suggested that m6A modification in mRNA and lncRNA is extremely widespread, and functionally modulates the eukaryotic transcriptome to influence RNA splicing, export, localization, translation, and stability (20–22). To study whether m6A modification exists in *FAM225A*, we first predicted the m6A sites located in *FAM225A* using an online bioinformatics tools m6Avar (http://m6avar.renlab.org/) and found 2 RRACU m6A sequence motifs in the last exon (at position 2,808 and 5,460). Next, we performed methylated RNA immunoprecipitation (Me-RIP) assays in 2 nasopharyngeal epithelial cells (NP69 and N2Tert) and 2 NPC cells (SUNE-1 and HONE-1). The results showed that the m6A level was higher in HONE-1 and SUNE-1 cells than that in NP69 and N2Tert cells (Fig. 1J). We then performed shRNA-mediated silencing of *METTL3*, a core component of m6A methylase complex (23), and found that downregulation of *METTL3* resulted in the decreased m6A level of both total RNA and *FAM225A* RNA (Supplementary Fig. S2A and S2B; Fig. 1K). We then investigated whether m6A modification could affect RNA metabolism of *FAM225A*. Knockdown of *METTL3* leads to approximately 50% to 60% lower expression of total *FAM225A* (Fig. 1L). We then measured the loss of *FAM225A* RNA after blocking new RNA synthesis with actinomycin D. The results indicated that *FAM225A* showed lower RNA stability after silencing of *METTL3* (Fig. 1M). These findings raise the possibility that the m6A level of *FAM225A* is higher in NPC, and m6A modification in *FAM225A* improved its transcripts stability, which may partially account for the significantly upregulation of *FAM225A* in NPC.

FAM225A promotes NPC cell proliferation, migration, and invasion

To investigate the potential role of *FAM225A* in NPC, we first performed GSEA based on the GSE12452 data set. This analysis showed significant enrichment of high *FAM225A* expression in gene sets related to cell proliferation and metastasis (Fig. 2A). To evaluate the influence of *FAM225A* on NPC cell proliferative and metastatic abilities, we transfected HNE-1 and SUNE-1 cells with 2 different shRNAs against *FAM225A* (sh-*FAM225A* 1# and sh-*FAM225A* 2#) or transfected NP69, N2Tert, HNE-1, and

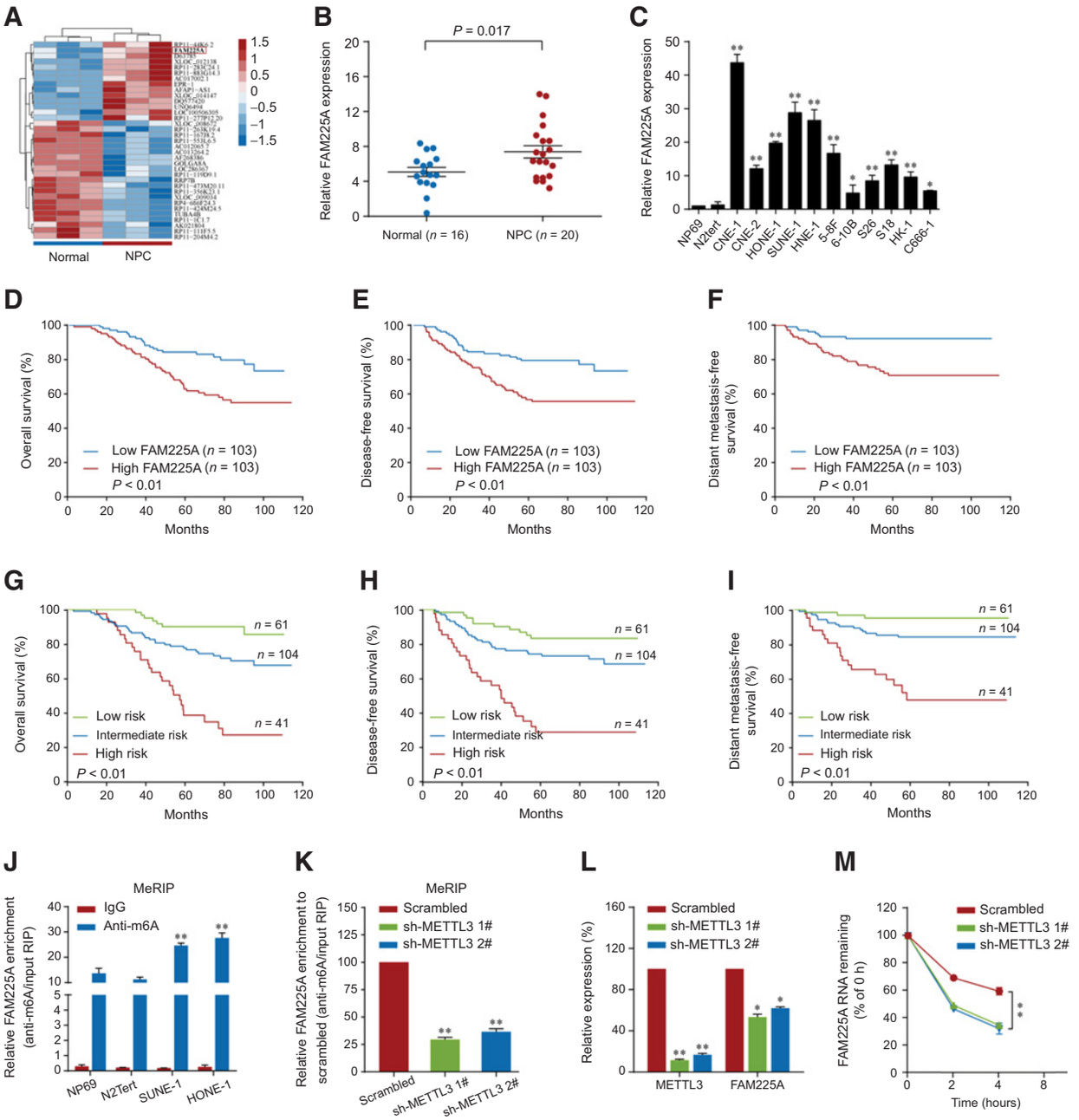

Figure 1.

m6A-modified *FAM225A* is overexpressed in NPC and is associated with poor clinical outcome. **A,** Heat map of the most differentially expressed lncRNAs between three pairs of NPC and normal nasopharynx tissues (fold change ≥ 2; $P < 0.05$ and raw signal intensity >1,500). **B,** Relative expression of *FAM225A* in NPC ($n = 20$) and normal nasopharyngeal epithelial tissues ($n = 16$). GAPDH was used as the endogenous control. Data represent the mean ± SEM. **C,** *FAM225A* expression level in the immortalized NP69 and N2Tert cells and 11 NPC cell lines. **D–F,** Kaplan–Meier analysis of the correlation between *FAM225A* expression and overall survival (**D**), disease-free survival (**E**), and distant metastasis-free survival (**F**) in a cohort of 206 NPC patients. **G–I,** Kaplan–Meier analysis of overall survival (**G**), disease-free survival (**H**), and distant metastasis-free survival (**I**) according to the NPC prognostic prediction model in patients with low-risk (*FAM225A* low expression and early TNM stage, $n = 61$), intermediate-risk (*FAM225A* high expression or advanced TNM stage, $n = 104$), and high-risk (*FAM225A* high expression and advanced TNM stage, $n = 41$) groups. **J,** m6A methylation level of *FAM225A* in normal nasopharyngeal epithelial cells (NP69 and N2Tert) and NPC cells (SUNE-1 and HONE-1) was determined by MeRIP-qPCR assays. **K,** Changes in m6A-modified *FAM225A* levels upon *METTL3* slicing. The input RNA fraction C_t value was used to account for RNA sample preparation differences, and negative control groups (IgG) were used to adjust background fraction. **L,** Transcript levels of *METTL3* and *FAM225A* in negative control and sh-*METTL3* SUNE-1 cells. **M,** Reduction of *FAM225A* RNA stability in *METTL3* knockdown SUNE-1 cells as compared with control. Cells were treated with 5 μg/mL actinomycin D and RNA was isolated at 0, 2, and 4 hours. Data represent the mean ± SD. *, $P < 0.05$; **, $P < 0.01$. The experiments were independently repeated at least three times.

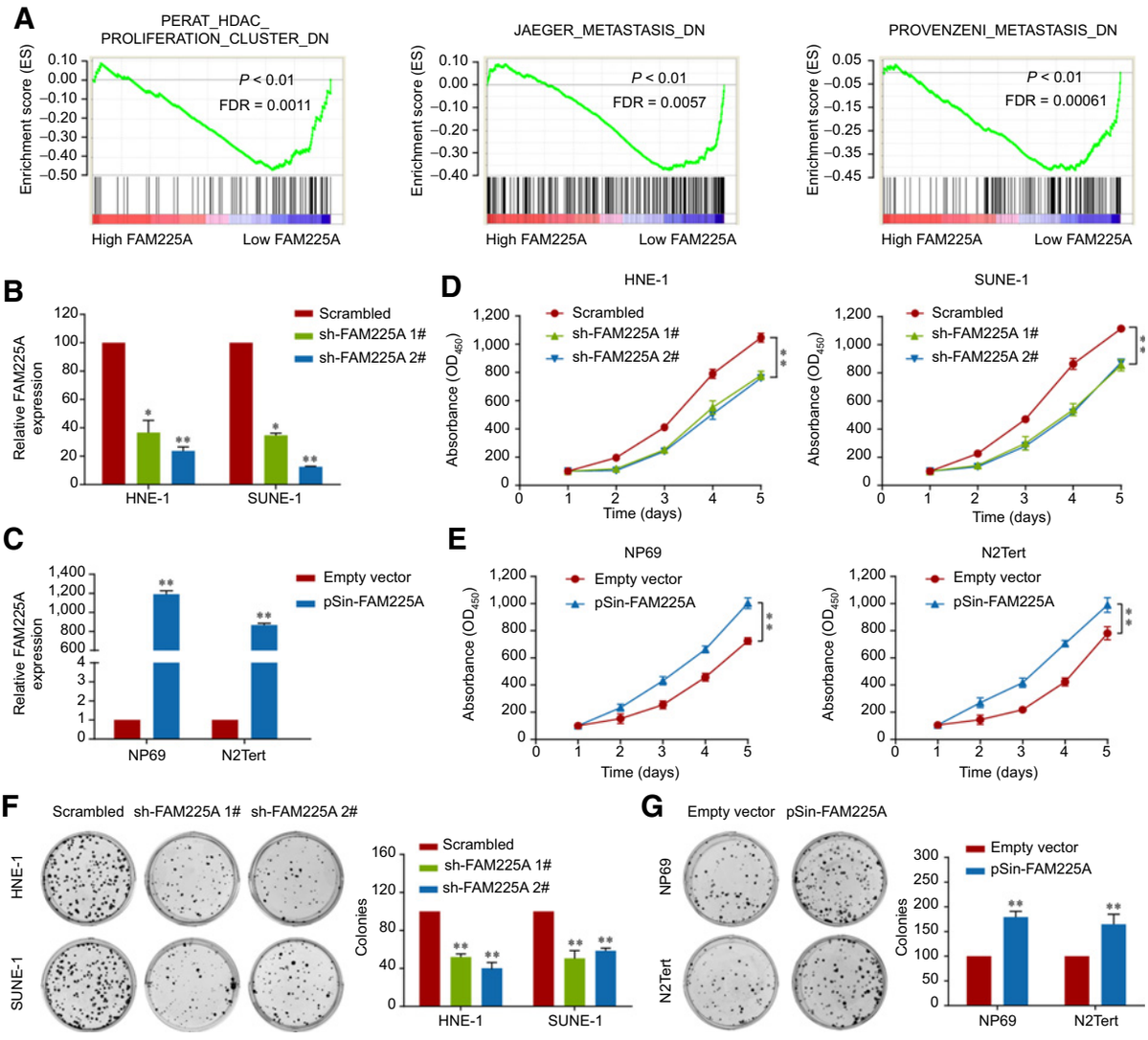

Figure 2.

FAM225A promotes NPC cell proliferation and colony formation. **A,** GSEA revealed that proliferation- and metastasis-related biological functions were enriched in response to high *FAM225A* expression based on the public GSE12452 data set. **B** and **C,** Expression of *FAM225A* in HNE-1 and SUNE-1 cells transfected with shRNA-*FAM225A*s or scrambled control (**B**) and in NP69 and N2Tert transfected with pSin-EF2-*FAM225A* or empty vector (**C**). **D,** CCK-8 assay of HNE-1 and SUNE-1 cells transfected with shRNA-*FAM225A*s or scrambled control. **E,** CCK-8 assay of NP69 and N2Tert cells transfected with pSin-EF2-*FAM225A* or empty vector. **F,** Representative images (left) and quantification (right) of the colony formation assay in HNE-1 and SUNE-1 cells transfected with shRNA-*FAM225A*s or scrambled control. **G,** Representative images (left) and quantification (right) of the colony formation assay of NP69 and N2Tert cells transfected with pSin-EF2-*FAM225A* or empty vector. Data represent the mean ± SD. *, $P < 0.05$; **, $P < 0.01$. The experiments were independently repeated at least three times.

SUNE-1 cells with a *FAM225A*-overexpressing plasmid (pSin-EF2-*FAM225A*) and confirmed the transfection efficiency by quantitative RT-PCR analysis (Fig. 2B and C). CCK-8 and colony formation assays revealed significant inhibition of growth and proliferation of NPC cells transfected with sh-*FAM225A* compared with those transfected with scrambled vectors, whereas the opposite effects were observed following *FAM225A* overexpression (Fig. 2 D–G; Supplementary Fig. S3A–S3C; all $P < 0.01$). Moreover, wound-healing and transwell assays showed that *FAM225A* silencing inhibited NPC cell migration and invasion (Fig. 3A and B, all $P < 0.01$). In contrast, *FAM225A* overexpression enhanced cell migration and invasion (Fig. 3C and D; Supplementary Fig. S3D and S3E; all $P < 0.01$). Taken together, these findings suggested that *FAM225A* functions as an oncogenic lncRNA in NPC.

FAM225A acts as a ceRNA and competitively absorbs miR-590-3p and miR-1275

To explore how *FAM225A* exerts its function, we predicted its subcellular localization by lncATLAS (http://lncatlas.crg.eu/). *FAM225A* was predicted to be located mainly in the cytoplasm of all the available cell types (Fig. 4A). Quantitative RT-PCR analysis of *FAM225A* in the nucleus and cytoplasm showed that *FAM225A* was localized mainly in the cytoplasm of NPC

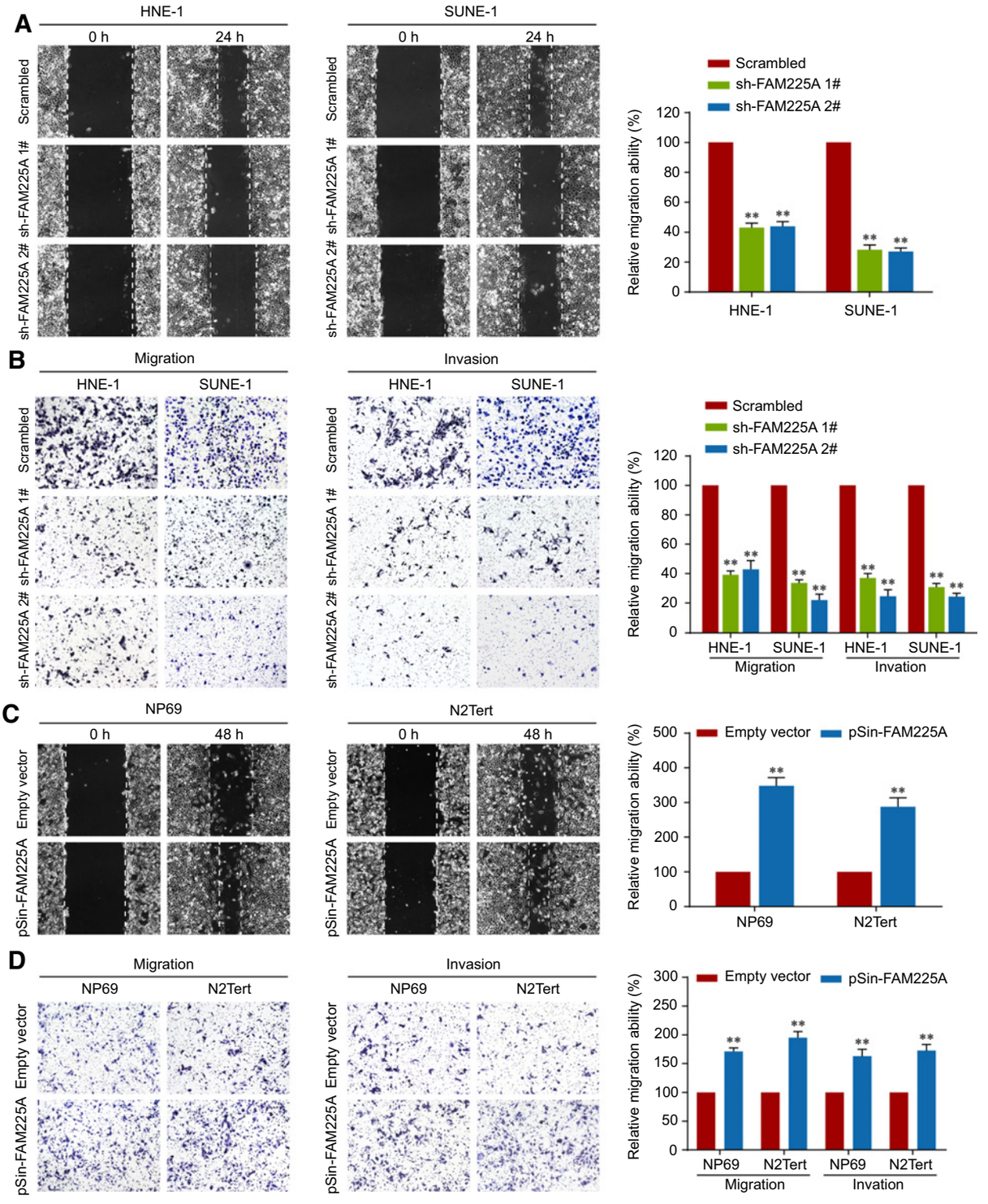

Figure 3.

FAM225A promotes NPC cell migration and invasion. **A,** Representative images (left) and quantification (right) of wound-healing assays in HNE-1 and SUNE-1 cells transfected with shRNA-*FAM225A*s or scrambled control. **B,** Representative images (left) and quantification (right) of transwell migration and invasion assays in HNE-1 and SUNE-1 cells transfected with shRNA-*FAM225A*s or scrambled control. **C,** Representative images (left) and quantification (right) of wound-healing assays in NP69 and N2Tert cells transfected with pSin-EF2-*FAM225A* or empty vector. **D,** Representative images (left) and quantification (right) of transwell migration and invasion assays in NP69 and N2Tert cells transfected with pSin-EF2-*FAM225A* or empty vector. Data represent the mean ± SD. **, $P < 0.01$. The experiments were independently repeated at least three times.

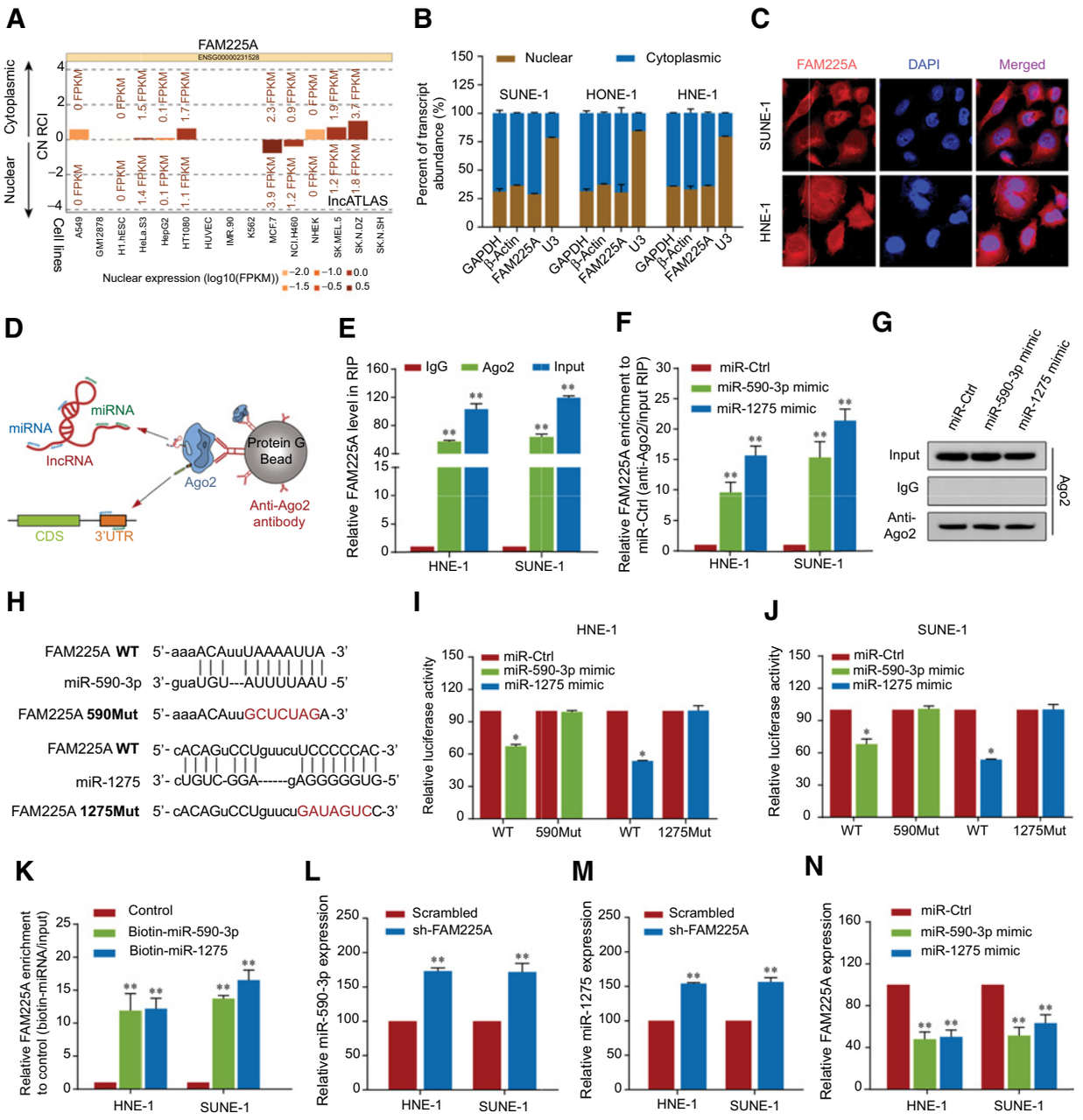

Figure 4.

FAM225A acts as a ceRNA and competitively absorbs miR-590-3p and miR-1275. **A,** *FAM225A* was predicted to be located mainly in the cytoplasm using the bioinformatics tools in lncATLAS. **B,** Quantitative RT-PCR analysis of subcellular *FAM225A* expression in the nucleus and cytoplasm of SUNE-1, HONE-1, and HNE-1 cells. GAPDH, β-actin, and U3 were used as endogenous controls. **C,** Subcellular localization of *FAM225A* in SUNE-1 and HNE-1 cells detected by RNA-FISH. *FAM225A*, red (Cy3); nuclei, blue (DAPI). **D,** Schematic diagram of the Ago2-RIP process. **E,** Fold enrichment of *FAM225A* in HNE-1 and SUNE-1. **F** and **G,** Enrichment of *FAM225A* in HNE-1 and SUNE-1 cells transfected with miR-590-3p, miR-1275 mimic, or miR-Ctrl (**F**). Ago2 protein immunoprecipitated by Ago2 antibody or IgG was detected by Western blot analysis (**G**). **H,** The predicted miR-590-3p and miR-1275 binding sites in the *FAM225A* transcript. The red nucleotides represent mutant sequences of target sites. **I** and **J,** The luciferase activities in HNE-1 (**I**) and SUNE-1 (**J**) cells cotransfected with WT or mutant (590Mut/1275Mut) *FAM225A* plasmid together with miR-590-3p or miR-1275 mimic or miR-Ctrl. **K,** Enrichment of *FAM225A* pulled down by biotin-miR-590-3p, biotin-miR-1275, or negative control. **L** and **M,** Relative levels of miR-590-3p (**L**) and miR-1275 (**M**) in HNE-1 and SUNE-1 cells transfected with sh-*FAM225A* #2 or scrambled control. **N,** Relative levels of *FAM225A* in HNE-1 and SUNE-1 cells transfected with miR-590-3p or miR-1275 mimics or miR-Ctrl. Data represent the mean ± SD. *, $P < 0.05$; **, $P < 0.01$. The experiments were independently repeated at least three times.

cells, which was verified by FISH assay (Fig. 4B and C; Supplementary Fig. S4A and S4B, $P < 0.05$). Based on these results, we hypothesized that *FAM225A* functions as a ceRNA. Because Ago2 is a core component of the RISC that participates in miRNA-mediating mRNA destabilization or translational repression, we conducted RIP assays using an anti-Ago2 antibody (Fig. 4D), which showed that endogenous *FAM225A* was preferentially enriched in Ago2-RIPs compared with control IgG-RIPs (Fig. 4E, $P < 0.01$). These findings suggested that *FAM225A* acts as a ceRNA to promote NPC cell development and progression.

We then predicted miRNAs that can bind with *FAM225A* using the publicly available DIANA Tools, and selected the top 30 miRNAs for further analysis (Supplementary Table S9). Ago-2-RIP assay showed that miR-590-3p and miR-1275 were the highest enriched miRNAs in the *FAM225A* overexpression group than in the vector group (Supplementary Fig. S5). To validate this, the Ago2-RIP assay also demonstrated that the *FAM225A* enrichment was much higher in miR-590-3p or miR-1275 overexpression groups than that in the miR-Ctrl group (Fig. 4F and G, $P < 0.01$), indicating that *FAM225A* and miR-590-3p/miR-1275 are in the same RISC. Next, using dual-luciferase reporter assays, we showed that overexpression of miR-590-3p or miR-1275 reduced luciferase activity of the wild-type *FAM225A* reporter gene, but not the *FAM225A*-590Mut or *FAM225A*-1275Mut vector (Fig. 4H–J, $P < 0.05$). Moreover, biotin-labeled miRNA pulldown assays showed markedly elevated *FAM225A* expression in NPC cells transfected with biotin-labeled miR-590-3p and miR-1275 compared with that in the control (Fig. 4K, $P < 0.01$). Finally, *FAM225A* silencing significantly increased the expression of miR-590-3p and miR-1275 (Fig. 4L and M, $P < 0.01$), whereas *FAM225A* expression was obviously suppressed by overexpression of miR-590-3p or miR-1275 (Fig. 4N, $P < 0.01$). Then, quantitative RT-PCR and ISH demonstrated that the expression of *FAM225A* was negatively correlated with miR-590-3p and miR-1275 expression (Supplementary Fig. S6A–S6C, $P < 0.001$). These results indicated that *FAM225A* directly "sponges" miR-590-3p and miR-1275.

We first transfected NP69 and N2Tert cells with miR-590-3p-inhibitor, miR-1275-inhibitor, and inhibitor control (Supplementary Fig. S7A) and found that silencing miR-590-3p and miR-1275 could promote the cell growth and proliferation (Supplementary Fig. S7B, all $P < 0.01$), as well as the migration and invasion (Supplementary Fig. S7C, all $P < 0.01$) of NP69 and N2Tert cells. These data indicated that silencing of miR-590-3p and miR-1275 endows NP69 and N2Tert cells with carcinogenicity *in vitro*. Furthermore, we investigated the involvement of miR-590-3p and miR-1275 in the mechanism by which *FAM225A* promotes NPC development and progression. NPC cells were cotransfected with pSin-EF2-*FAM225A* plasmids together with miR-590-3p/miR-1275 mimics. *In vitro* function experiments revealed that the proliferative, migratory, and invasive abilities of NPC cells were obviously suppressed by overexpression of miR-590-3p or miR-1275, which further reversed the ability of *FAM225A* overexpression to promote the proliferative, migratory, and invasive abilities of NPC cells (Supplementary Fig. S8A–S8J, $P < 0.01$). These results suggested that the carcinogenic effect of *FAM225A* is partially mediated by negative regulation of miR-590-3p and miR-1275.

FAM225A decoys miR-590-3p and miR-1275 to upregulate their common target, ITGB3

To find out genes sharing the regulatory role of miR-590-3p and miR-1275 with *FAM225A*, we first predicted the common target genes of miR-590-3p and miR-1275 using TargetScan. Among the predicted target genes, the integrin family genes (such as *ITGA1*, *ITGA3*, *ITGA11*, *ITGB3*, etc.) caught our attention because our previous study reported that the integrin family genes play important roles in NPC progression (24, 25). Then, we found that only *ITGB3* could be affected by the modulation of miR-590-3p/miR-1275 expression (Fig. 5A and B, $P < 0.01$); thus, it was selected for further analysis. Luciferase reporter assays showed that overexpression of miR-590-3p, miR-1275, or both repressed luciferase activity in NPC cells transfected with the wild-type (WT) *ITGB3* 3′-UTR reporter plasmid, whereas no obvious inhibition was observed in cells transfected with the mutant reporter plasmid (Fig. 5C–E). Furthermore, Biotin-labeled miRNA pulldown assays verified that *ITGB3* is the target gene of miR-590-3p and miR-1275 (Fig. 5F, $P < 0.01$).

Further investigations showed that upregulation and downregulation of *FAM225A* positively affected *ITGB3* expression at both the mRNA and protein levels (Fig. 5G and H, $P < 0.01$). We also detected a positive correlation between *FAM225A* and *ITGB3* expression in NPC based on the GEO data set (GSE12452, Fig. 5I, $P < 0.001$), which was also found in 12 other cancer types in TCGA database (Supplementary Fig. S9). These findings indicated the existence of a *FAM225A*-miR-590-3p/miR-1275-*ITGB3* regulatory axis.

ITGB3 has been reported to promote tumorigenesis by activating the FAK/PI3K/Akt pathway (26, 27). Therefore, we investigated the ability of modulation of the *FAM225A*-miR-590-3p/miR-1275-ITGB3 axis to influence FAK/PI3K/Akt pathway activation. *FAM225A* silencing decreased *ITGB3* protein levels and the phosphorylation levels of FAK (p-FAK) and Akt (p-Akt); these effects were partially reversed by cotransfection with miR-590-3p/miR-1275 inhibitors (Fig. 5J). In contrast, *FAM225A* overexpression increased *ITGB3* protein levels and the phosphorylation levels of FAK (p-FAK) and Akt (p-Akt), effects that were partially reversed by cotransfection with miR-590-3p/miR-1275 mimics (Fig. 5K). These findings indicated that *FAM225A* decoys miR-590-3p and miR-1275 to upregulate their common target *ITGB3* and activate the FAK/PI3K/Akt pathway.

ITGB3 is responsible for FAM225A-mediated cell proliferation, migration, and invasion

To verify the ability of *FAM225A* to promote tumor progression in an *ITGB3*-dependent manner, we transfected HNE-1 and SUNE-1 cells stably expressing sh-*FAM225A* or scrambled vector with the *ITGB3*-overexpression vector or the corresponding empty vector. *In vitro* function experiments demonstrated that restoration of *ITGB3* expression partially rescued the suppressive effects of *FAM225A* knockdown on NPC cell proliferation, migration, and invasion (Fig. 6A–G, $P < 0.01$). Moreover, rescue experiments showed that *ITGB3* overexpression increased the phosphorylation levels of FAK and Akt inhibited by *FAM225A* downregulation, whereas as *ITGB3* knockdown had the opposite effect (Fig. 6H and I).

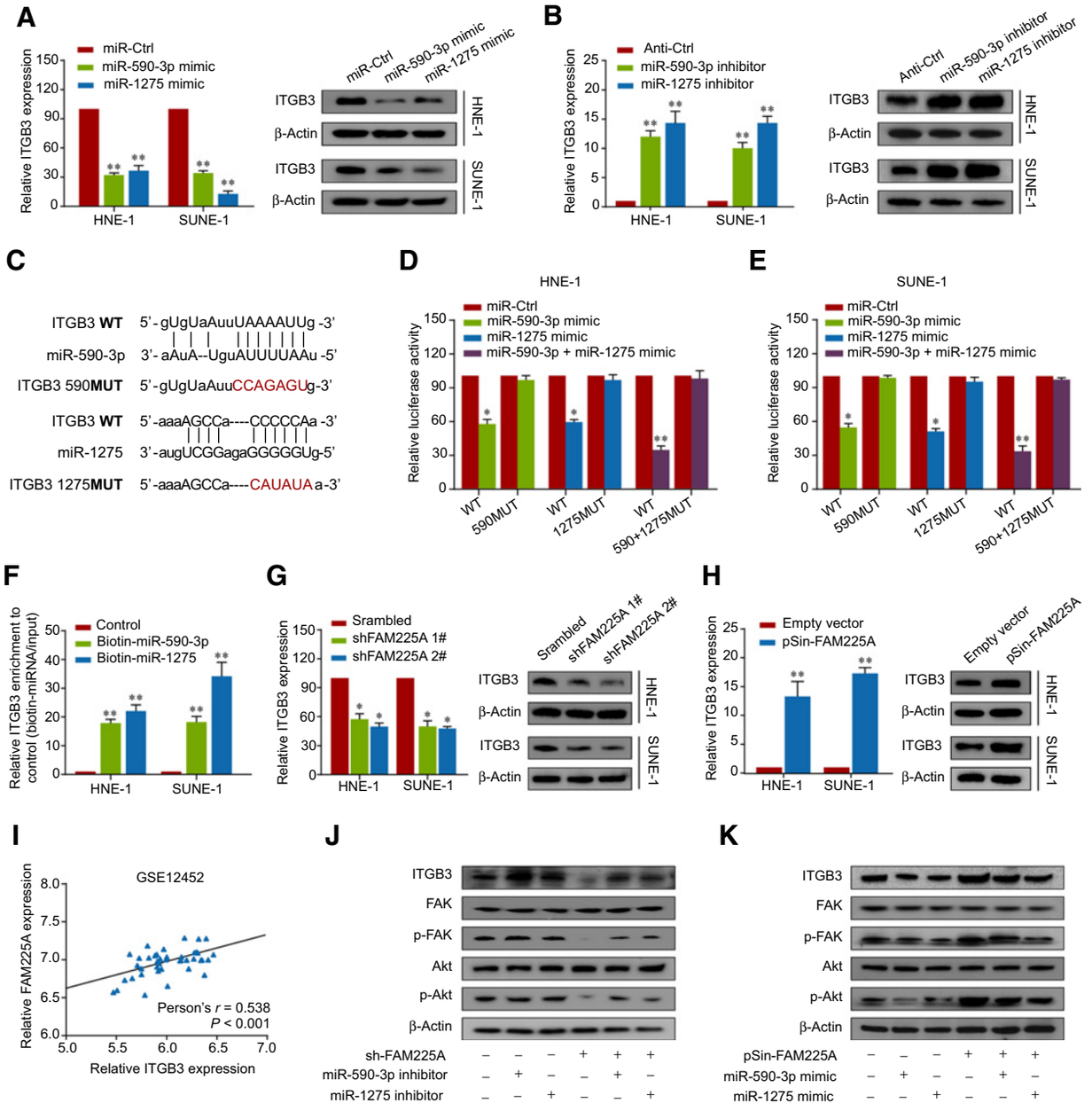

Figure 5.

FAM225A functions as a decoy for miR-590-3p and miR-1275 to increase *ITGB3* expression. **A,** Relative mRNA and protein levels of *ITGB3* in HNE-1 and SUNE-1 cells transfected with miR-590-3p or miR-1275 mimics or miR-Ctrl. **B,** Relative mRNA and protein levels of *ITGB3* in HNE-1 and SUNE-1 cells transfected with miR-590-3p or miR-1275 inhibitor or anti-Ctrl. **C,** The predicted binding sites of miR-590-3p and miR-1275 in the 3′-UTR of *ITGB3*. The red nucleotides represent mutant sequences of target sites. **D** and **E,** Luciferase activities in HNE-1 (**D**) and SUNE-1 (**E**) cells cotransfected WT or mutant (590Mut/1275Mut) *ITGB3* plasmid together with miR-590-3p or miR-1275 mimic or miR-Ctrl. **F,** Enrichment of *ITGB3* pulled down by biotin-labeled miR-590-3p, biotin-labeled miR-1275, or negative control. **G** and **H,** Relative mRNA and protein levels of *ITGB3* in HNE-1 and SUNE-1 cells transfected with sh-*FAM225A*s or its scrambled control (**G**), as well as pSin-EF2-*FAM225A* or its empty vector (**H**). **I,** Correlation between *FAM225A* and *ITGB3* expression based on the GEO database (GSE12452). **J,** Expression of *ITGB3* and phosphorylation levels of FAK (p-FAK) and Akt (p-Akt) in cells cotransfected with sh*FAM225A* #2 or scrambled control together with miR-590-3p or miR-1275 inhibitor. **K,** Expression of *ITGB3*, p-FAK, and p-Akt in cells cotransfected with psin-EF2-*FAM225A* or empty vector together with miR-590-3p or miR-1275 mimic. Data represent the mean ± SD. *, $P < 0.05$; **, $P < 0.01$. The experiments were independently repeated at least three times.

These findings demonstrated that *FAM225A* is an oncogenic lncRNA that promotes NPC cell proliferation, migration, and invasion via the *FAM225A*-miR-590-3p/miR-1275-*ITGB3*-FAK/PI3K/Akt signaling pathway (Fig. 6J).

FAM225A promotes NPC cell tumorigenesis and metastasis *in vivo*

We then confirmed the ability of *FAM225A* to promote NPC proliferation and metastasis in *vivo*. The tumor growth model

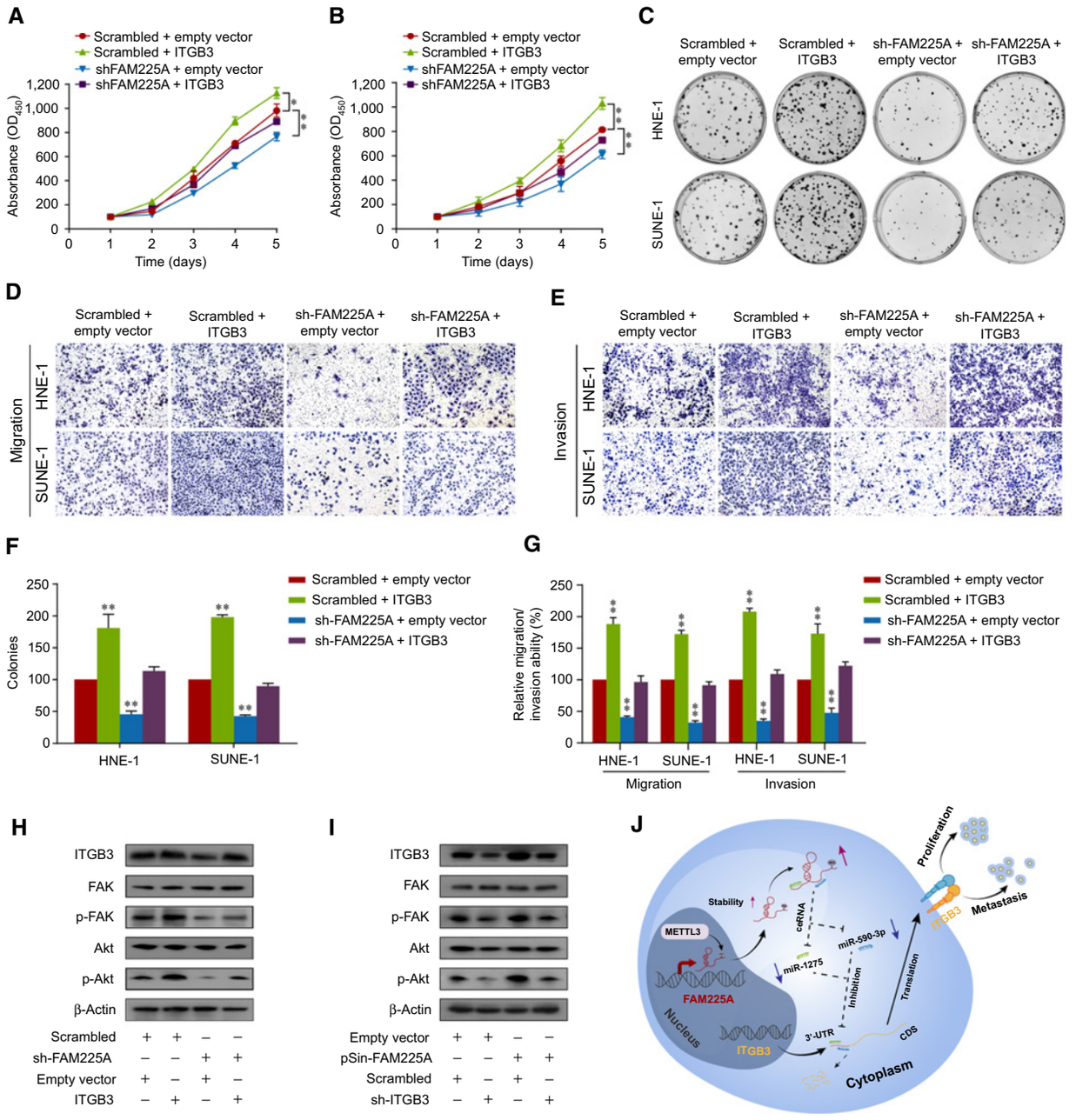

Figure 6.

ITGB3 is responsible for *FAM225A*-mediated proliferation, migration, and invasion. **A** and **B,** CCK-8 assay of HNE-1 (**A**) and SUNE-1 (**B**) cells cotransfected with sh*FAM225A* #2 or scrambled control together with psin-EF2-*ITGB3* or empty vector. **C,** Representative images (left) and quantification (right) of the colony formation assay in the above-mentioned NPC cells. **D–G,** Representative images and quantification of transwell migration and invasion assays in the above-mentioned NPC cells. **H,** Western blot analysis of *ITGB3*, FAK, p-FAK, Akt, p-Akt in the NPC cells cotransfected with sh*FAM225A* #2 or scrambled control together with pENTER-*ITGB3* or empty vector. **I,** Western blotting analysis of *ITGB3*, FAK, p-FAK, Akt, p-Akt in HNE-1 and SUNE1 cells cotransfected with pSin-EF2-*FAM225A* or empty vector together with sh-*ITGB3* or scrambled control. **J,** Proposed model of the mechanism underlying the expression and function of *FAM225A* in NPC cell proliferation and metastasis. Data represent mean ± SD. *, $P < 0.05$; **, $P < 0.01$. The experiments were independently repeated at least three times.

showed that *FAM225A* knockdown significantly inhibited tumor growth (Fig. 7A–C, $P < 0.05$). Moreover, quantitative RT-PCR, ISH and IHC assays confirmed that *FAM225A* knockdown resulted in downregulation of *ITGB3* expression (Fig. 7D and E). The lung metastasis model showed that the number of macroscopic and microscopic metastatic nodules formed in lungs was significantly lower in the *FAM2225A* knockdown group (Fig. 7F and G, Supplementary Fig. S10A, $P < 0.05$). In addition, using the

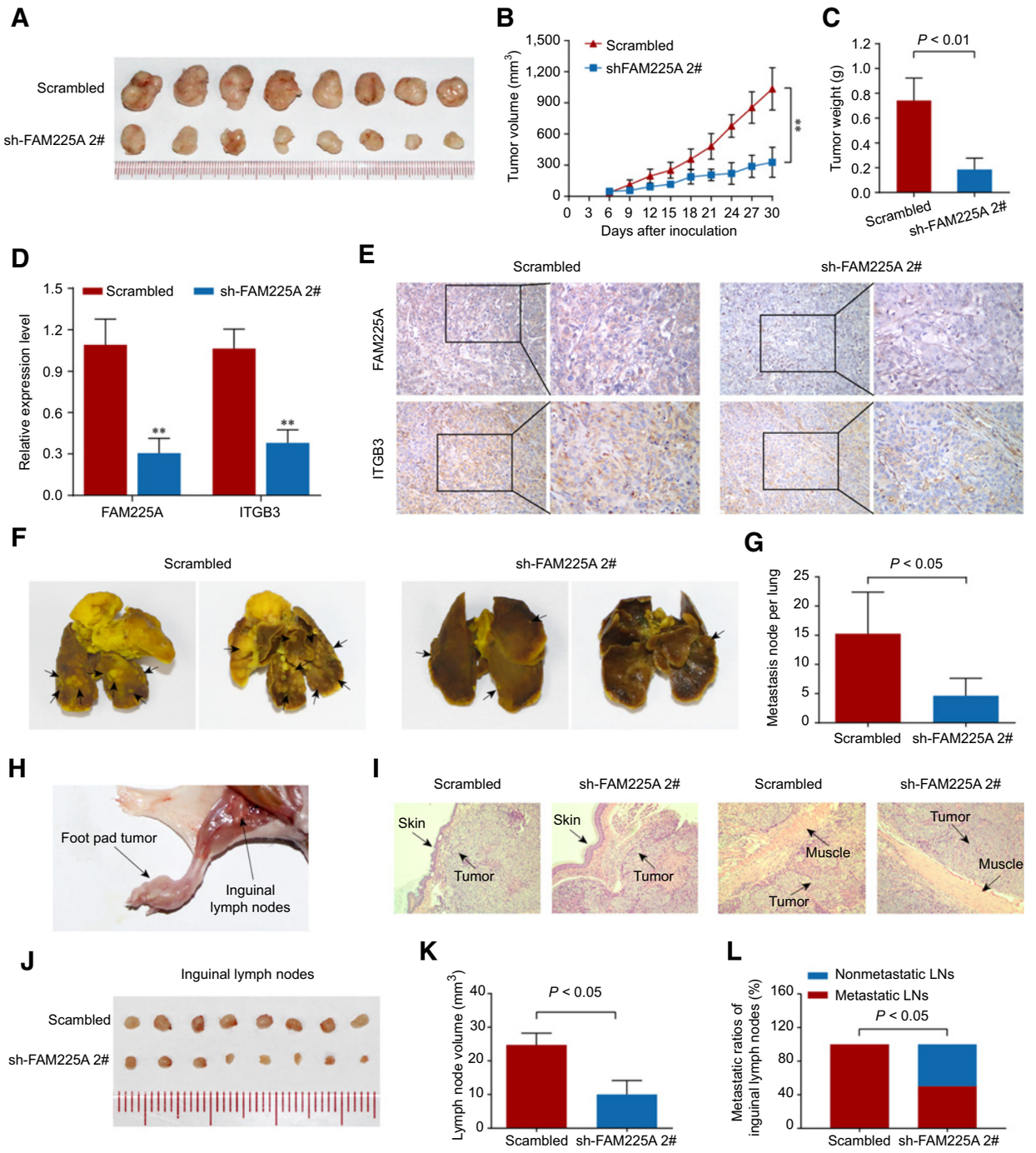

Figure 7.

FAM225A promotes NPC cell tumorigenesis and metastasis *in vivo*. **A–C,** HNE-1 cells stably expressing sh-*FAM225A* #2 or scrambled control were transplanted into the axilla of nude mice to construct tumor growth model. Representative images (**A**), tumor volume growth curves (**B**), and weight (**C**) of the formed tumors. **D** and **E,** *FAM225A* and *ITGB3* expression in tumors detected by quantitative RT-PCR (**D**), *ISH* and IHC (**E**). **F** and **G,** SUNE-1 cells stably expressing sh-*FAM225A* #2 or scrambled control were injected into the tail vein of mice to construct a lung metastasis model. Representative images (**F**) and quantification (**G**) of macroscopic metastatic nodules on lung surfaces. **H–L,** SUNE1 cells stably expressing sh-*FAM225A* #2 or scrambled control were injected into footpads of mice to construct an inguinal lymph node metastasis model. Representative images of the primary foot pad tumor and metastatic inguinal lymph node (**H**) and the microscopic primary tumors in footpads following hematoxylin and eosin staining (**I**); representative images (**J**) and quantification (**K**) of the volumes of the inguinal lymph nodes, and metastatic ratios of inguinal lymph nodes (**L**). Data represent mean ± SD. **, $P < 0.01$.

inguinal lymph node metastatic model (Fig. 7H), we found that the tumors in the sh-*FAM225A* group were less aggressive in terms of invasion toward the skin and muscle (Fig. 7I). Moreover, the volumes of the inguinal lymph nodes were smaller, with fewer pan-cytokeratin–positive tumor cells in the *FAM225A* knockdown group (Fig. 7J and K). Strikingly, the inguinal lymph node metastasis ratio was markedly lower in the *FAM225A* knockdown group (Fig. 7L; Supplementary Table S10; Supplementary Fig. S10B–S10D). Finally, we found that restoration of *ITGB3* expression partially rescued the suppressive effects of *FAM225A* knockdown on tumor growth and metastasis (Supplementary Fig. S11A–S11F; Supplementary Table S10). These data suggested that *FAM225A* contributes to NPC tumorigenesis and metastasis *in vivo*.

Discussion

Accumulating evidence indicates that lncRNAs dysregulation plays important roles in the tumorigenesis and progression of various types of cancers. Here, we found that lncRNA *FAM225A* was obviously upregulated and associated with worse survival in NPC. *FAM225A* promoted NPC cell growth and metastasis *in vitro* and *in vivo* by acting as a ceRNA to sponge miR-590-3p/miR-1275, leading to increased *ITGB3* expression. These findings suggest that *FAM225A* plays a carcinogenic role in the occurrence and development of NPC and may be used as a prognostic indicator in NPC patients.

In the clinic, the risk of recurrence or distant metastasis in NPC patients cannot be precisely distinguished by the current anatomic-based TNM staging system. Thus, the large variation in the clinical outcomes of NPC patients calls for novel prognostic biomarkers. Emerging evidence suggests that lncRNAs might serve as novel prognostic indicators (28). In this study, we also detected *FAM225A* expression levels in paraffin-embedded NPC tissue samples by quantitative RT-PCR for risk stratification and prognostic prediction. Although nucleic acids are extensively degraded in paraffin-embedded tissues, they are still valuable assets for clinical translational research. Thus, we used primers to generate short *FAM225A* amplicons (approximately 60 bp) for the enhancement of the quantification efficiency and reliability as previously described (29–30). Survival analysis revealed that NPC patients with a high *FAM225A* expression had worse clinical outcomes, indicating the potential of *FAM225A* as a promising prognostic biomarker to guide the development of personalized therapies for NPC patients.

The m6A modification is widespread throughout the transcriptome, accounting for about 0.2% of total adenosine of cellular RNA (31). The dynamic and reversible modification of m6A installed and erased by N6-methyltransferases (such as *METTL3*, *METTL14*, and *KIAA1429*, etc.) and demethylases (such as *FTO* and *ALKBH5*) regulates gene expression and cell fate (32). m6A modification has been shown to participate in the occurrence and development of various cancers (33–35). The fate of m6A-modified RNA depends on the function of the different proteins that identify them, which has impacts on stability, translation efficiency, secondary structure, subcellular localization, and alternative polyadenylation (36–38). Here, we found that m6A is enriched on *FAM225A* in NPC cells. Modification of m6A in *FAM225A* leads to the improvement of its RNA stability, which may partially account for upregulation of *FAM225A* in NPC. In addition to m6A modification, there might exist other mechanisms that are involved in the elevation of *FAM225A*, such as DNA methylation, histone modification, and miRNA dysregulation (39–41), which deserve further exploration.

Growing evidence supports the existence of a novel and extensive interaction network involving ceRNAs (42–45), in which lncRNAs regulate miRNAs by competitively binding their target sites on protein-coding mRNA molecules. For example, LINC01234 functions as a ceRNA to regulate CBFB expression by sponging miR-204-5p to promote gastric cancer cell proliferation (42), DANCR functions as a ceRNA to promote ROCK1-mediated proliferation and metastasis by acting as a decoy for miR-335-5p and miR-1972 in osteosarcoma (46), and UICLM promotes colorectal cancer metastasis by acting as a ceRNA that sponges miRNA-215 to regulate ZEB2 expression (47). In this study, we found that *FAM225A* was located mainly in the cytoplasm of NPC cells, and acted as a sponge for miR-590-3p and miR-1275.

MiR-590-3p is reported to be downregulated in various types of cancers and functions as a tumor suppressor miRNA (48, 49). Moreover, lncRNA UCA1 is reported to function as a ceRNA to enhance CREB1 expression by competitively sponging miR-590-3p in gastric cancer (50). In addition, miR-1275 is reported not only to suppress G_1/S transition via inhibition of HOXB5 and thus suppress NPC cell growth (28), but also to inhibit hepatocellular carcinoma cell growth by simultaneously regulating IGF2BPs and IGF1R (51). Our findings reveal the significance of the interaction between *FAM225A* and miR-590-3p/miR-1275 in tumorigenesis. *FAM225A* plays a carcinogenic role in NPC by promoting cell proliferation and metastasis, which can be partially rescued by overexpression of miR-590-3p or miR-1275.

In general, as a ceRNA, the function of lncRNAs depends on the miRNA target. Using an online database, we predicted *ITGB3* as a potential target of both miR-590-3p and miR-1275, which was confirmed by luciferase reporter and biotin-labeled miRNA pulldown assays. Furthermore, overexpression of miR-590-3p or miR-1275 inhibited *ITGB3* mRNA and protein expression. *ITGB3* belongs to the family of integrins, which are transmembrane receptors that mediate intercellular and extracellular matrix binding and promote signal transduction via the PI3K and MAPK pathways. Integrin heterodimers, comprising α and β subunits, regulate cell proliferation, survival, and migration, predominantly via focal adhesion kinase and Src kinase family members (52, 53). *ITGB3* has been reported to be associated with tumor aggression and metastasis by activating FAK and Akt signaling (26, 54). In the present study, we demonstrated that *FAM225A* upregulates *ITGB3* expression and activates the FAK/PI3K/AKT signaling pathway by competitively sponging miR-590-3p and miR-1275, thus promoting NPC cell proliferation and metastasis.

In conclusion, we identified *FAM225A* as an oncogenic lncRNA in NPC. Functional and mechanistic analyses revealed that *FAM225A* promotes NPC cell proliferation, migration, and invasion by acting as a ceRNA that sponges miR-590-3p and miR-1275, leading to enhanced *ITGB3* expression and activation of the FAK/PI3K/Akt pathway. Our study demonstrates that *FAM225A* plays an important role in NPC tumorigenesis and progression, and highlights its importance as a prognostic indicator and promising therapeutic target in NPC.

Disclosure of Potential Conflicts of Interest

No potential conflicts of interest were disclosed.

Authors' Contributions

Conception and design: Z.-Q. Zheng, Z.-X. Li, G.-Q. Zhou, FP Chen, J. Zhang N. Liu, Y. Sun
Development of methodology: Z.-Q. Zheng, G.-Q. Zhou, X. Wen, Y.-Q. Li, N. Liu, Y. Sun
Acquisition of data (provided animals, acquired and managed patients, provided facilities, etc.): Z.-Q. Zheng, Z.-X. Li, L.-L. Zhang, X.-D. Huang, R.-Q. Liu, J. Kou, X. Wen, N. Liu
Analysis and interpretation of data (e.g., statistical analysis, biostatistics, computational analysis): Z.-Q. Zheng, Z.-X. Li, L.-L. Zhang, J.-W. Lv, X.-J. He, X. Wen
Writing, review, and/or revision of the manuscript: Z.-Q. Zheng, Z.-X. Li, G.-Q. Zhou, J.-W. Lv, J. Zhang, Y.-Q. Li, N. Liu, Y. Sun
Administrative, technical, or material support (i.e., reporting or organizing data, constructing databases): G.-Q. Zhou, N. Liu, Y. Sun
Study supervision: Z.-Q. Zheng, Z.-X. Li, L. Lin, J. Ma, Y. Sun

Acknowledgments

This work was supported by grants from the National Natural Science Foundation of China (No. 81872463 and 81773229), the Health and Medical Collaborative Innovation Project of Guangzhou City, China (No. 201604020003 and 201803040003), the Special Support Program of Sun Yat-sen University Cancer Center (16zxtzlc06), the Natural Science Foundation of Guangdong Province (No. 2017A030312003), the Innovation Team Development Plan of the Ministry of Education (No. IRT_17R110), and the National Key R&D Program of China (2016YFC0902000). The key raw data have been uploaded to Research Data Deposit public platform (www.researchdata.org.cn), with an approval number of RDDB2019000555.

The costs of publication of this article were defrayed in part by the payment of page charges. This article must therefore be hereby marked *advertisement* in accordance with 18 U.S.C. Section 1734 solely to indicate this fact.

Received March 11, 2019; revised June 4, 2019; accepted July 11, 2019; published first July 22, 2019.

References

1. Wei KR, Zheng RS, Zhang SW, Liang ZH, Li ZM, Chen WQ. Nasopharyngeal carcinoma incidence and mortality in China, 2013. Chinese J Cancer 2017; 36:90.
2. Bray F, Ferlay J, Soerjomataram I, Siegel RL, Torre LA, Jemal A. Global cancer statistics 2018: GLOBOCAN estimates of incidence and mortality worldwide for 36 cancers in 185 countries. CA Cancer J Clin 2018;68: 394–424.
3. Wei F, Wu Y, Tang L, Xiong F, Guo C, Li X, et al. Trend analysis of cancer incidence and mortality in China. Science China-Life Sciences 2017;60: 1271–5.
4. Sun Y, Li WF, Chen NY, Zhang N, Hu GQ, Xie FY, et al. Induction chemotherapy plus concurrent chemoradiotherapy versus concurrent chemoradiotherapy alone in locoregionally advanced nasopharyngeal carcinoma: a phase 3, multicentre, randomised controlled trial. Lancet Oncology 2016;17:1509–20.
5. Lai SZ, Li WF, Chen L, Luo W, Chen YY, Liu LZ, et al. How does intensity-modulated radiotherapy versus conventional two-dimensional radiotherapy influence the treatment results in nasopharyngeal carcinoma patients? Int J Radiat Oncol Biol Phys 2011;80:661–8.
6. Guo R, Tang LL, Mao YP, Du XJ, Chen L, Zhang ZC, et al. Proposed modifications and incorporation of plasma Epstein-Barr virus DNA improve the TNM staging system for Epstein-Barr virus-related nasopharyngeal carcinoma. Cancer 2019;125:79–89.
7. Tang XR, Li YQ, Liang SB, Jiang W, Liu F, Ge WX, et al. Development and validation of a gene expression-based signature to predict distant metastasis in locoregionally advanced nasopharyngeal carcinoma: a retrospective, multicentre, cohort study. Lancet Oncology 2018;19:382–93.
8. Liu N, Chen NY, Cui RX, Li WF, Li Y, Wei RR, et al. Prognostic value of a microRNA signature in nasopharyngeal carcinoma: a microRNA expression analysis. Lancet Oncology 2012;13:633–41.
9. Quinn JJ, Chang HY. Unique features of long non-coding RNA biogenesis and function. Nat Rev Genet 2016;17:47–62.
10. Mondal T, Juvvuna PK, Kirkeby A, Mitra S, Kosalai ST, Traxler L, et al. Sense-antisense lncRNA pair encoded by locus 6p22.3 determines neuroblastoma susceptibility via the USP36-CHD7-SOX9 regulatory axis. Cancer Cell 2018;33:417–34.
11. Poliseno L, Salmena L, Zhang J, Carver B, Haveman WJ, Pandolfi PP. A coding-independent function of gene and pseudogene mRNAs regulates tumour biology. Nature 2010;465:1033–8.
12. Mercer TR, Dinger ME, Mattick JS. Long non-coding RNAs: insights into functions. Nat Rev Genet 2009;10:155–9.
13. Huarte M. The emerging role of lncRNAs in cancer. Nat Med 2015;21: 1253–61.
14. Seiler J, Breinig M, Caudron-Herger M, Polycarpou-Schwarz M, Boutros M, Diederichs S. The lncRNA VELUCT strongly regulates viability of lung cancer cells despite its extremely low abundance. Nucleic Acids Res 2017; 45:5458–69.
15. Zhang E, Han L, Yin D, He X, Hong L, Si X, et al. H3K27 acetylation activated-long non-coding RNA CCAT1 affects cell proliferation and migration by regulating SPRY4 and HOXB13 expression in esophageal squamous cell carcinoma. Nucleic Acids Res 2017;45:3086–101.
16. The lncRNA NORAD contributes to the maintenance of genomic stability. Cancer Discov 2018;8:1209.
17. Wen X, Tang X, Li Y, Ren X, He Q, Yang X, et al. Microarray expression profiling of long non-coding RNAs involved in nasopharyngeal carcinoma metastasis. Int J Mol Sci 2016;17:1956.
18. Ørom UA, Lund AH. Isolation of microRNA targets using biotinylated synthetic microRNAs. Methods 2007;43:162–5.
19. Phatak P, Donahue JM. Biotinylated Micro-RNA pull down assay for identifying miRNA targets. Bio-protocol 2017;7:e2253.
20. Choe J, Lin S, Zhang W, Liu Q, Wang L, Ramirez-Moya J, et al. mRNA circularization by METTL3-eIF3h enhances translation and promotes oncogenesis. Nature 2018;561:556–60.
21. Deng X, Su R, Weng H, Huang H, Li Z, Chen J. RNA N(6)-methyladenosine modification in cancers: current status and perspectives. Cell Res 2018;28: 507–17.
22. Huang H, Weng H, Sun W, Qin X, Shi H, Wu H, et al. Recognition of RNA N(6)-methyladenosine by IGF2BP proteins enhances mRNA stability and translation. Nat Cell Biol 2018;20:285–95.
23. Wang X, Feng J, Xue Y, Guan Z, Zhang D, Liu Z, et al. Structural basis of N (6)-adenosine methylation by the METTL3-METTL14 complex. Nature 2016;534:575–8.
24. Zhang J, Zheng ZQ, Yuan YW, Zhang PP, Li YQ, Wang YQ, et al. NFAT1 hypermethylation promotes epithelial-mesenchymal transition and metastasis in nasopharyngeal carcinoma by activating ITGA6 transcription. Neoplasia 2019;21:311–21.
25. Tang X, Wen X, He Q, Li Y, Ren X, Yang X, et al. MicroRNA-101 inhibits invasion and angiogenesis through targeting ITGA3 and its systemic delivery inhibits lung metastasis in nasopharyngeal carcinoma. Cell Death Dis. 2017;8:e2566.
26. Naik A, Al-Yahyaee A, Abdullah N, Sam JE, Al-Zeheimi N, Yaish MW, et al. Neuropilin-1 promotes the oncogenic Tenascin-C/integrin beta3 pathway and modulates chemoresistance in breast cancer cells. BMC Cancer 2018; 18:533.
27. Zhang N, Ma D, Wang L, Zhu X, Pan Q, Zhao Y, et al. Insufficient radiofrequency ablation treated hepatocellular carcinoma cells promote metastasis by up-regulation ITGB3. J Cancer 2017;8:3742–54.
28. Sun KY, Peng T, Chen Z, Huang J, Zhou XH. MicroRNA-1275 suppresses cell growth, and retards G_1/S transition in human nasopharyngeal carcinoma by down-regulation of HOXB5. J Cell Commun Signal 2016;10: 305–14.
29. Kong H, Zhu M, Cui F, Wang S, Gao X, Lu S, et al. Quantitative assessment of short amplicons in FFPE-derived long-chain RNA. Sci Rep 2014;47246.

30. Carninci P. Molecular biology: the long and short of RNAs. Nature 2009; 457:974–5.
31. Yang D, Qiao J, Wang G, Lan Y, Li G, Guo X, et al. N6-Methyladenosine modification of lincRNA 1281 is critically required for mESC differentiation potential. Nucleic Acids Res 2018;46:3906–20.
32. Zhang S, Zhao BS, Zhou A, Lin K, Zheng S, Lu Z, et al. m(6)A demethylase ALKBH5 maintains tumorigenicity of glioblastoma stem-like cells by sustaining FOXM1 expression and cell proliferation program. Cancer Cell 2017;31:591–606.
33. Winkler R, Gillis E, Lasman L, Safra M, Geula S, Soyris C, et al. m(6)A modification controls the innate immune response to infection by targeting type I interferons. Nat Immunol 2019;20:173–82.
34. Dorn LE, Lasman L, Chen J, Xu X, Hund TJ, Medvedovic M, et al. The N(6)-methyladenosine mRNA methylase METTL3 controls cardiac homeostasis and hypertrophy. Circulation 2019;139:533–45.
35. Wang Y, Li Y, Yue M, Wang J, Kumar S, Wechsler-Reya RJ, et al. N(6)-methyladenosine RNA modification regulates embryonic neural stem cell self-renewal through histone modifications. Nat Neurosci 2018;21: 195–206.
36. Molinie B, Wang J, Lim KS, Hillebrand R, Lu ZX, Van Wittenberghe N, et al. m(6)A-LAIC-seq reveals the census and complexity of the m(6)A epitranscriptome. Nat Methods 2016;13:692–8.
37. Zheng G, Dahl JA, Niu Y, Fedorcsak P, Huang CM, Li CJ, et al. ALKBH5 is a mammalian RNA demethylase that impacts RNA metabolism and mouse fertility. Mol Cell 2013;49:18–29.
38. Liu N, Dai Q, Zheng G, He C, Parisien M, Pan T. N(6)-methyladenosine-dependent RNA structural switches regulate RNA-protein interactions. Nature 2015;518:560–4.
39. Wang Z, Yang B, Zhang M, Guo W, Wu Z, Wang Y, et al. lncRNA epigenetic landscape analysis identifies EPIC1 as an oncogenic lncRNA that interacts with MYC and promotes cell-cycle progression in cancer. Cancer Cell 2018; 33:706–20.
40. Zhang E, He X, Zhang C, Su J, Lu X, Si X, et al. A novel long noncoding RNA HOXC-AS3 mediates tumorigenesis of gastric cancer by binding to YBX1. Genome Biol 2018;19:154.
41. Ma MZ, Zhang Y, Weng MZ, Wang SH, Hu Y, Hou ZY, et al. Long noncoding RNA GCASPC, a target of miR-17–3p, negatively regulates pyruvate carboxylase-dependent cell proliferation in gallbladder cancer. Cancer Res 2016;76:5361–71.
42. Chen X, Chen Z, Yu S, Nie F, Yan S, Ma P, et al. Long noncoding RNA LINC01234 functions as a competing endogenous RNA to regulate CBFB expression by sponging miR-204–5p in gastric cancer. Clin Cancer Res 2018;24:2002–14.
43. Yu C, Li L, Xie F, Guo S, Liu F, Dong N, et al. LncRNA TUG1 sponges miR-204-5p to promote osteoblast differentiation through upregulating Runx2 in aortic valve calcification. Cardiovasc Res 2018;114: 168–79.
44. Salmena L, Poliseno L, Tay Y, Kats L, Pandolfi PP. A ceRNA hypothesis: the Rosetta Stone of a hidden RNA language? Cell 2011;146:353–8.
45. Thomson DW, Dinger ME. Endogenous microRNA sponges: evidence and controversy. Nat Rev Genet 2016;17:272–83.
46. Wang Y, Zeng X, Wang N, Zhao W, Zhang X, Teng S, et al. Long noncoding RNA DANCR, working as a competitive endogenous RNA, promotes ROCK1-mediated proliferation and metastasis via decoying of miR-335-5p and miR-1972 in osteosarcoma. Mole Cancer 2018;17:89.
47. Chen DL, Lu YX, Zhang JX, Wei XL, Wang F, Zeng ZL, et al. Long non-coding RNA UICLM promotes colorectal cancer liver metastasis by acting as a ceRNA for microRNA-215 to regulate ZEB2 expression. Theranostics 2017; 7:4836–49.
48. Zu C, Liu S, Cao W, Liu Z, Qiang H, Li Y, et al. MiR-590-3p suppresses epithelial-mesenchymal transition in intrahepatic cholangiocarcinoma by inhibiting SIP1 expression. Oncotarget 2017;8: 34698–708.
49. Ge X, Gong L. MiR-590-3p suppresses hepatocellular carcinoma growth by targeting TEAD1. Tumour Biol 2017;39:1393393717.
50. Gu L, Lu LS, Zhou DL, Liu ZC. UCA1 promotes cell proliferation and invasion of gastric cancer by targeting CREB1 sponging to miR-590–3p. Cancer Med 2018;7:1253–63.
51. Fawzy IO, Hamza MT, Hosny KA, Esmat G, El TH, Abdelaziz AI. miR-1275: a single microRNA that targets the three IGF2-mRNA-binding proteins hindering tumor growth in hepatocellular carcinoma. FEBS Lett 2015;589: 2257–65.
52. Guan JL. Role of focal adhesion kinase in integrin signaling. Int J Biochem Cell Biol 1997;29:1085–96.
53. Vuori K, Hirai H, Aizawa S, Ruoslahti E. Introduction of p130cas signaling complex formation upon integrin-mediated cell adhesion: a role for Src family kinases. Mol Cell Biol 1996;16:2606–13.
54. Wendt MK, Schiemann WP. Therapeutic targeting of the focal adhesion complex prevents oncogenic TGF-beta signaling and metastasis. Breast Cancer Res 2009;11:R68.